

# Mechanisms driving shape distortion in two-dimensional flow

A. DE CHAUMONT QUITRY, D. H. KELLEY and N. T. OUELLETTE<sup>(a)</sup>

*Department of Mechanical Engineering & Materials Science, Yale University - New Haven, CT 06520, USA*

received 1 April 2011; accepted in final form 10 May 2011

published online 10 June 2011

PACS 47.27.T – Turbulent transport processes

PACS 47.52.+j – Chaos in fluid dynamics

PACS 47.27.De – Coherent structures

**Abstract** – In order to elucidate the physical processes governing the evolution of material areas in complex flow, we study the shape dynamics of three-point Lagrangian clusters in an experimental quasi-two-dimensional flow. By comparing our measurements with simulations of triangles evolving purely diffusively, we show that the path taken by the mean triangle shape through a suitably defined phase space is indicative of the underlying flow dynamics. We demonstrate the existence of organizing curves in shape space for the evolution of triangles with different initial shapes. Our results suggest a detailed, multi-step process governing the shape dynamics of clusters in complex flow.

Copyright © EPLA, 2011

**Introduction.** – The advection of passive scalar fields by fluid flows with complex spatiotemporal structure is relevant in a wide range of natural and industrial situations [1]. When the Péclet number, which compares the importance of advection and scalar diffusion, is large, the dynamics of the scalar concentration are pinned to the fluid flow, and isocontours of the scalar field are stretched and folded just as fluid material volumes are. For that reason, a characterization of the Lagrangian dynamics of the flow field, and in particular the evolution of material volumes, is necessary to understand the advection of scalar fields.

Material volumes themselves can be parametrized by a cluster of discrete fluid elements [2–4]. In general, a minimum of  $d + 1$  fluid elements is required to describe a  $d$ -dimensional structure; that is, a three-dimensional material volume requires four points (often known as a “tetrad” [2]), while a two-dimensional material area requires three points. Such minimal parameterizations are the basis of a class of turbulent-flow models [2,5], which have motivated several experimental and numerical studies of multi-particle clusters in turbulence [6–8].

In previous work [9], we showed that the shapes assumed by triangles advected in a two-dimensional spatiotemporally chaotic fluid flow mirrored those observed in turbulent flows, suggesting that fully developed energy cascades are not required to produce strongly distorted shapes. We found that the most important factor in determining the

triangle shape distribution was the *size* of the triangles, but that the multi-scale nature of the Eulerian flow field was not the reason for this dependence.

Here, we extend our previous work by studying the detailed mechanisms that drive the deformation of Lagrangian triangles in an effort to connect the observed shapes with the flow dynamics. After describing our experimental setup and the ways in which we characterize triangle shapes, we discuss how the shape distributions of initially equilateral triangles evolve with time. We subsequently consider the role of the initial triangle shape, and find not only that all initial conditions converge to the same ultimate shape distribution but also that there are several preferred paths through the space of triangle shapes that organize the dynamics. We contrast our results with simulations of triangles evolving under purely diffusive dynamics (that is, in the limit of very low Peclet number), which show very different shape dynamics. These results lead us to a mechanistic picture of triangle deformation in our flow field. Finally, we show how the shape evolution can be explained by considering the topological structure of the flow field. We finish by summarizing and discussing the connections between our results and the more general turbulent-flow problem.

**Methodology.** – As we have described elsewhere [9–11], our apparatus generates quasi-two-dimensional flow via electromagnetic forcing. We place a thin layer, 4 mm deep, of an electrolyte (14% by mass NaCl in water) above an array of permanent magnets. The magnets are

<sup>(a)</sup>E-mail: nicholas.ouellette@yale.edu

arranged in a square lattice of alternating polarity, with a center-to-center spacing of  $L_f = 2.54$  cm, which we take to be the forcing scale. The fluid is separated from the magnets by a glass plate with a thickness of 3.18 mm; the glass is coated with a hydrophobic wax to reduce bottom-friction effects. The entire flow cell measures  $86 \times 86$  cm<sup>2</sup> ( $34L_f \times 34L_f$ ), of which we measure the central  $31 \times 23$  cm<sup>2</sup> ( $12L_f \times 9L_f$ ), and contains 1156 magnets. The unusually large size of the apparatus allows us to measure long-time Lagrangian statistics, ensures that the effects of the lateral side walls are negligible in the measurement area, and provides a wide range of scales larger than the forcing scale  $L_f$ .

In order to drive fluid flow, we run DC electric current (of order 1 A) through the electrolyte. The combination of the horizontal current density and the vertical magnetic field leads to a Lorentz body force on the fluid, which sets it into motion [12–16]. The spatiotemporal structure of the flow field is characterized by the Reynolds number  $\text{Re} = u' L_f / \nu$ , where  $u'$  is the root-mean-square velocity (of order 1 cm/s) and  $\nu$  is the kinematic viscosity. For  $\text{Re} \lesssim 70$ , the flow field is a square lattice of steady vortices of alternating sign. As  $\text{Re}$  increases, the symmetries of this cellular flow are spontaneously broken and the flow becomes chaotic in space and time [16,17]. Eventually, at  $\text{Re} \approx 200$ , the vertical velocity profile becomes unstable and the flow develops a non-negligible component in the depth direction [11]. Here, we report results at  $\text{Re} = 185$  (driven by a forcing current of 1.5 A), well above the transition to chaos but still in the quasi-two-dimensional regime. Though we do observe some inverse energy transfer, our flow does not exhibit a fully developed inverse energy cascade.

To measure the flow fields, we use particle tracking velocimetry (PTV). Briefly, we seed the fluid with  $51 \mu\text{m}$  fluorescent polystyrene microspheres; these particles are less dense than the electrolyte, and so float to its surface. To minimize surface-tension-driven interactions among the particles, we float an additional thin layer of fresh water above the electrolyte. The particles sit on the (miscible) interface between these two fluids. We image the particles with a 4-megapixel camera at a frame rate of 60 Hz. Estimating the time scale of the forcing to be  $T_L = L_f / u' \sim 2$  s, this frame rate gives us a time resolution of 167 samples per  $T_L$ . We image roughly 35 000 particles per frame, locating them with a precision of about 0.1 pixels ( $\sim 13 \mu\text{m}$ ); the mean interparticle spacing is on the order of 15 particle diameters. We then track the motion of the particles using a three-frame predictive algorithm [18], and differentiate the resulting particle tracks by convolving them with a Gaussian smoothing and differentiating filter [19], giving us a set of locations and velocities at each time step. To suppress noise and ensure that these fields are two-dimensional, we project the measurements onto a set of numerically computed stream function eigenmodes [11,20]. Finally, we construct virtual Lagrangian trajectories (thereby avoiding potential finite-volume bias

from long measured trajectories [21]) by numerically solving the equations of motion for fluid elements given the measured fields using a second-order Runge-Kutta integrator [9,14,15,22].

To describe the shapes and sizes of Lagrangian triangles, we label their side lengths as  $\Lambda_1$ ,  $\Lambda_2$ , and  $\Lambda_3$ , with  $\Lambda_1 \geq \Lambda_2 \geq \Lambda_3$ , and their internal angles as  $\theta_1$ ,  $\theta_2$ , and  $\theta_3$ , with  $\theta_1 \geq \theta_2 \geq \theta_3$ . We characterize the size of a triangle with the radius of gyration, given by

$$R_g^2 = \frac{1}{3}(\Lambda_1^2 + \Lambda_2^2 + \Lambda_3^2). \quad (1)$$

We are primarily interested, however, in the triangle shape. The shape has two degrees of freedom, and so we require two independent parameters to characterize it. One common choice is to define the vectors  $\boldsymbol{\rho}_1 \equiv (\mathbf{r}_2 - \mathbf{r}_1) / \sqrt{2}$  and  $\boldsymbol{\rho}_2 \equiv (2\mathbf{r}_3 - \mathbf{r}_2 - \mathbf{r}_1) / \sqrt{6}$ , where  $\mathbf{r}_n$  is the position of the  $n$ -th triangle vertex [23,24]. With these vectors, the parameters  $\chi \equiv (1/2) \arctan[2\boldsymbol{\rho}_1 \cdot \boldsymbol{\rho}_2 / (\rho_2^2 - \rho_1^2)]$  and  $w \equiv 2|\boldsymbol{\rho}_1 \times \boldsymbol{\rho}_2| / (\rho_1^2 + \rho_2^2)$  can then be defined to characterize the triangle shapes [3,4,13,25]. Unfortunately, although  $\chi$  and  $w$  are indeed independent quantities that are only functions of the triangle shape, they do not have clear geometric interpretations [13]. We therefore instead describe the triangle shape using a simpler set of parameters [9]: the largest internal angle  $\theta_1$  and the ratio of the smallest side to the intermediate side,  $\gamma \equiv \Lambda_3 / \Lambda_2$ , which gives a measure of the closeness of the nearest two vertices. Defined in this way,  $\theta_1 \in [\pi/3, \pi]$  and  $\gamma \in [0, 1]$ . We note that only shapes where  $\gamma \geq 2 \cos \theta_1$  are geometrically allowed.

**Results.** – As a Lagrangian triangle evolves under the action of flow, the shape of the three-point cluster changes and the mean triangle shape will move on some path through the shape space spanned by  $\gamma$  and  $\theta_1$ . When the evolution time is large compared to the correlation time of the flow field and the radius of gyration of the triangles has grown large compared to the correlation length of the field, the shape distribution will approach a universal form [3,9]. This “random” limit can be computed by considering the shapes assumed by triplets of uniformly distributed random numbers, and is given by  $\gamma = 0.55$  and  $\theta_1 = 0.65\pi$  for an unconstrained system like ours. The mean shape of a given population of triangles therefore has two well-defined limits: the initial shape distribution and the final random limit. The dynamics of the advecting field determine only the path joining these two points in shape space.

To illustrate this point, we show in fig. 1 the trajectories in shape space taken by two populations of initially equilateral ( $\gamma = 1$ ,  $\theta_1 = \pi/3$ ) triangles: one that is advected in our chaotic flow and one where the dynamics of the triangle vertices are simply diffusive. The ensemble of diffusive triangles moves rapidly and monotonically through shape space to its final distribution. The ensemble of chaotically advected triangles, however, shows markedly different

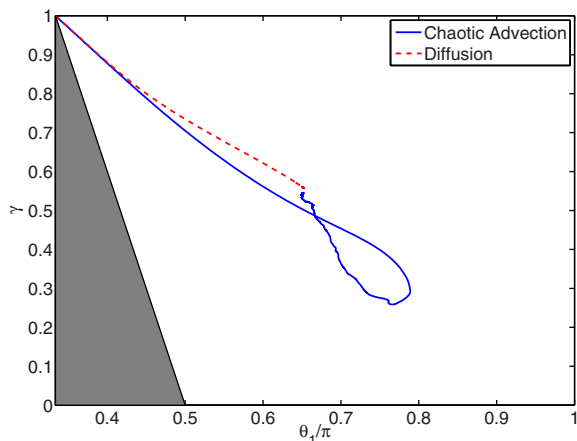


Fig. 1: (Color online) Mean shape of a population of initially small ( $R_g(t=0) = L_f/20$ ), equilateral ( $\gamma = 1, \theta_1 = \pi/3$ ) triangles, evolving either diffusively or in our experimental flow. Both populations begin and end at the same points in shape space, but take different paths in between.

behavior, exploring an intermediate, highly distorted regime before finally settling back to the random limit (after a time of roughly  $90T_L$ ). This type of “overshoot” has been observed previously [13,25], and was interpreted as a signature of turbulent flow. As we showed, however, robust turbulence cascades are not required for the development of such an overshoot [9]; rather, chaotic advection appears to be sufficient. Interestingly, we found that the triangle shapes were closely tied to the triangle sizes: large triangles favored shapes close to the random limit, while small triangles were more strongly distorted. These observations are scale-dependent and hold regardless of how long the triangles have evolved in time. We find that the shape statistics for each length scale are stationary. Triangle growth and deformation are therefore strongly coupled.

To gain more insight into the flow dynamics governing triangle shape and the connection with triangle size, we studied not only the mean triangle shapes but also the full shape distributions as a function of instantaneous triangle size. We advected a population of initially small triangles ( $R_g(t=0) = L_f/20$ ) until the mean triangle shape reached the random limit. We did not vary *initial* triangle size because previous work has shown that initially large triangles do not exhibit an overshoot, more closely tracking diffusive dynamics [9]. In fig. 2, we plot joint probability density functions (PDFs) of  $\gamma$  and  $\theta_1$  for four different ranges of instantaneous triangle size for the same chaotically advected triangles illustrated in fig. 1. The PDFs are computed using all triangles with appropriate sizes, regardless of when they reached those sizes. Accumulating shape data over time is justified here because the distributions are stationary. For very small triangles (fig. 2(a)), nearly all the triangles are equilateral. Since the triangles tend to grow rapidly as

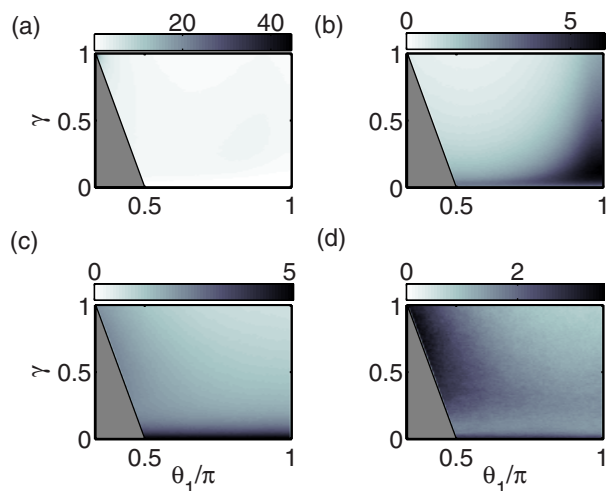


Fig. 2: (Color online) Joint probability density functions (PDFs) of  $\gamma$  and  $\theta_1$  of triangles advected in our chaotic flow. The PDFs are conditioned on triangle size, with (a)  $R_g/L_f < 10^{-1}$ , (b)  $10^{-1} \leq R_g/L_f < 10^{-1/4}$ , (c)  $10^{-1/4} \leq R_g/L_f < 10^{1/2}$ , and (d)  $10^{1/2} < R_g/L_f$ .

they are advected [9], the only triangles in this size range are those that have not yet had time to evolve, and so the PDF simply reflects the initial conditions. The PDFs for larger sizes, however, are determined by the flow dynamics. From fig. 2(b) and (c), it appears that the distortion of triangles at intermediate scales (that is, large compared to the initial triangle size but small compared to  $L_f$ , the forcing scale of the flow) can be decomposed into two distinct stages. First, the triangles are strongly strained, leading to a distribution that favors points that are close to collinear (large  $\theta_1$ ) and with two vertices much closer to each other than they are to the third (low  $\gamma$ ). Subsequently, this third vertex is rapidly advected away in a random direction, leading to a distribution that favors two vertices close together ( $\gamma \approx 0$ ) but that does not indicate any special internal angles. As the triangles continue to grow, the two close points begin to separate. Finally, once the triangles are large, the PDF becomes less strongly peaked, and favors shapes that are closer to equilateral, with a lower  $\theta_1$  and an intermediate  $\gamma$ .

When the triangles evolve diffusively rather than under the influence of chaotic advection, the picture is markedly different. The PDF changes rapidly from a delta function at the initial conditions to the stationary distribution shown in fig. 3. The similarity of the PDFs in fig. 2(d) and 3 is striking but expected: once the triangles are large, the motion of the three vertices is uncorrelated even in chaotic advection, and effectively they diffuse relative to each other.

Although most studies have considered shapes that are initially equilateral [8,9,13,25], this initial condition is somewhat arbitrary, since (as shown above) triangles rapidly distort into shapes that are far from isotropic.

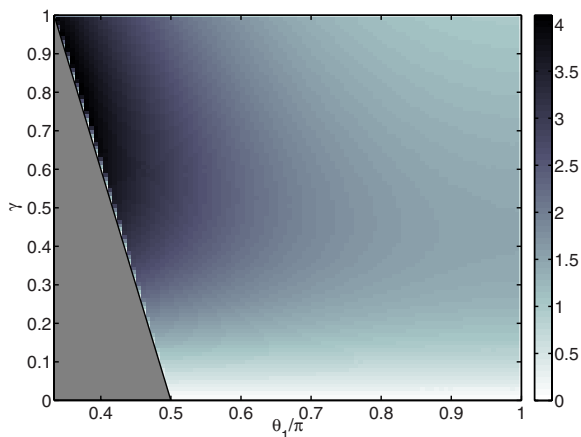


Fig. 3: (Color online) Joint probability density function (PDF) of  $\gamma$  and  $\theta_1$  for triangles that evolve diffusively. Contrary to the chaotic advection case, this PDF is independent of the triangle size. Note the close similarity between this PDF and the case of very large advected triangles (fig. 2(d)).

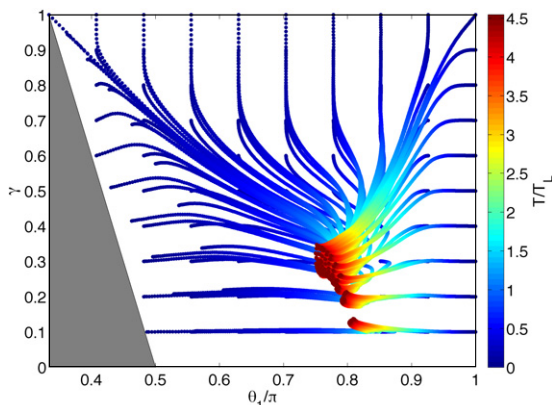


Fig. 4: (Color online) Trajectories of the mean triangle shape under chaotic advection for different initial conditions. Initially equilateral triangles deform much more quickly than those that are initially distorted, but all the ensembles approach the random limit at long times (and large sizes). Note the apparent existence of attracting curves onto which many different initial conditions quickly converge.

We therefore considered the effect of changing these initial conditions on the subsequent triangle evolution.

Figure 4 shows the paths of the mean shape taken in phase space by many different ensembles of triangles that began with different initial shapes. Just as for the initially equilateral case, all the ensembles distort away from their initial distribution and eventually converge to the random limit at long times. But rather than approaching this random limit in a different way for each initial condition, fig. 4 shows a surprising amount of self-organization in shape space. In particular, two special trajectories are apparent that appear to attract triangles with different initial conditions: one that begins in the upper left corner of the phase space (equilateral triangles)

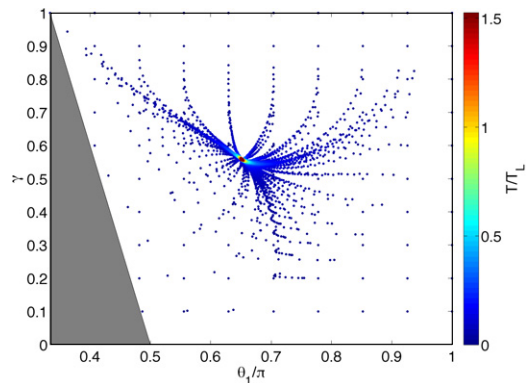


Fig. 5: (Color online) Trajectories of the mean triangle shape for diffusively evolving triangles, for different initial conditions. Unlike the chaotic advection case (fig. 4), diffusive triangles converge to the random limit very rapidly and without any clear organizing structure in shape space.

and sweeps towards the central part ( $\gamma \approx 0.4$ ,  $\theta_1/\pi \approx 0.75$ ) and one that begins in the upper right corner (equidistant collinear vertices). This result suggests, interestingly, that the detailed initial shape distribution of the triangles does not dominate the subsequent evolution, but rather that the flow dynamics impose structure on the shape changes and may be responsible for the presence of attracting curves in the phase-space flow. Predicting these organizing curves from the equations of motion remains an open challenge.

To clarify these suggestions, we also considered the effect of different initial conditions on diffusively evolving triangles, as shown in fig. 5. Unlike the case of chaotic advection, the diffusive triangles flow much more directly towards the random limit, and much less organization is evident.

In figs. 4 and 5, the triangles grow as they deform and move along the measured paths in shape space. As we showed previously, however, shape and size are tightly coupled [9]. Separating the two effects—that is, growth and deformation—can lead to a deeper understanding of the dynamics. To that end, we calculated both the triangle growth rate, defined as  $dR_g/dt$ , and the triangle deformation rate, defined as

$$\sqrt{\left(\frac{\partial\gamma}{\partial t}\right)^2 + \left(\frac{\partial\theta_1/\pi}{\partial t}\right)^2}. \quad (2)$$

The deformation rate is thus the magnitude of the rate of change of position in shape space. In fig. 6, we show the growth rate and deformation rate as a function of triangle shape for several different times. As is clearly shown, the triangles that *grow* quickly are not necessarily the same as those that *deform* quickly. The fastest-growing triangles are those that have large  $\gamma$  and are nearly collinear. Though the growth rate distributions are not stationary, this tendency persists at all times. Such quickly growing, collinear triangles are likely those that

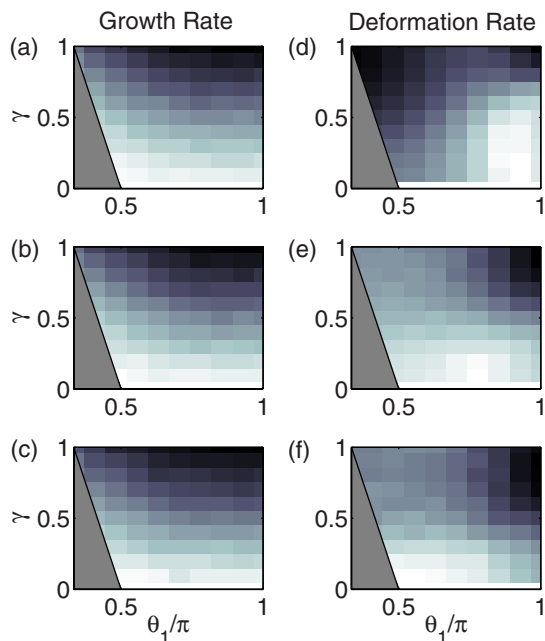


Fig. 6: (Color online) Rates of triangle growth (a)–(c) and deformation (d)–(f) for  $T/T_L = 3/4$  (a), (d), 1 (b), (e), and  $5/4$  (c), (f). In all cases, dark areas denote faster rates than light areas. Triangles that grow quickly are not necessarily those that deform quickly.

are trapped in strongly stretching Lagrangian Coherent Structures (LCS) [26], which are nearly line-like themselves [14]. Small collinear triangles should behave similarly to material-line segments, which have been shown to align strongly with the attracting LCS [27].

In contrast to the growth rate distributions, the distribution of triangles that deform the fastest is much more dependent on time. At short times, the most rapidly deforming triangles are those that are nearly equilateral, whereas low- $\gamma$ , high- $\theta_1$  triangles deform slowly. As time progresses, however, it is the high- $\gamma$ , high- $\theta_1$  triangles that deform quickly, while the slowly deforming triangles are those with low  $\gamma$  and low  $\theta_1$ .

These data, combined with the results shown in fig. 2, support a detailed, mechanistic picture for how triangles (and therefore material areas) evolve in our flow. Small triangles, regardless of their initial shape, are rapidly distorted into nearly collinear structures by the action of coherent (Lagrangian) strain. As these strained triangles are trapped in strongly stretching, line-like regions of the flow, they grow rapidly until they are large enough that the different vertices can sample distinct regions of the flow field. A single vertex is then typically swept away from the other two in a random direction, leading to triangles with low  $\gamma$  but random  $\theta_1$ . As the triangles continue to grow, the closer two vertices may also be separated, leading to shapes that move away from the extreme values of  $\gamma$  and  $\theta_1$ . Finally, once the three vertices are separated by distances large compared to the correlation length

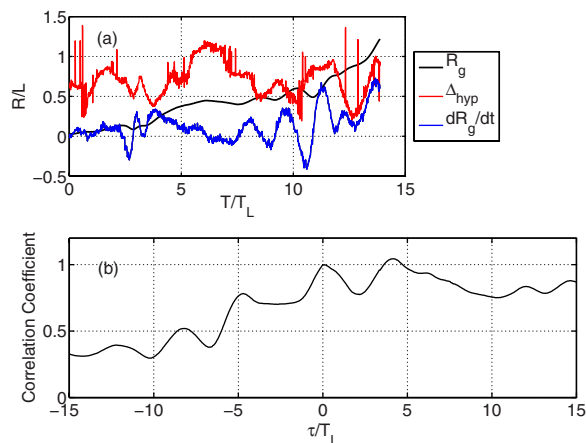


Fig. 7: (Color online) (a) Size ( $R_g$ ), growth rate ( $dR_g/dt$ ), and distance to the nearest hyperbolic point ( $\Delta_{hyp}$ ) for a single triangle. (b) Correlation coefficient of  $dR_g/dt$  and  $\Delta_{hyp}$  for the same triangle.

of the flow field, the vertices simply diffuse relative to one another and the distribution reaches the stationary, random limit.

To test the hypothesis that it is the coherent strain in the flow that drives the distortion and growth of triangles, we studied triangles as they passed near the hyperbolic critical points in our flow. The hyperbolic points are stagnation points that are purely straining, and drive much of the chaotic advection in the flow [28]. Previously, we introduced a robust algorithm for locating these points in experimental flow fields based on the curvature of Lagrangian trajectories [16,17], and showed that the hyperbolic points can sometimes be long-lived, particularly at lower Reynolds numbers. As the hyperbolic points are both sites of large, coherent strain and are the endpoints of LCS, they should have measurable effects on triangle shape if our hypotheses above are correct.

In fig. 7, we show data for an example triangle. As time evolves,  $R_g$  increases and the triangle grows more or less monotonically larger. The growth rate  $dR_g/dt$ , however, shows large fluctuations. To explain these fluctuations, we also plot the distance  $\Delta_{hyp}$  between the triangle centroid and the nearest hyperbolic point. Qualitatively, it appears that jumps in the growth rate are associated with times when the triangle centroid moves close to the hyperbolic point. This observation is supported by the cross-correlation of the two curves, shown in fig. 7(b): the two curves are strongly correlated.

A single triangle, however, can only tell us so much. We therefore computed the cross-covariance of  $\Delta_{hyp}$  and  $dR_g/dt$  for many triangles, as shown in fig. 8. In addition, we conditioned these covariances on  $R_g/L_{hyp}$ , where  $L_{hyp}$  is the mean hyperbolic point spacing, by truncating the trajectories of triangles that exceed this threshold. Two features are evident from these plots. First,  $\Delta_{hyp}$

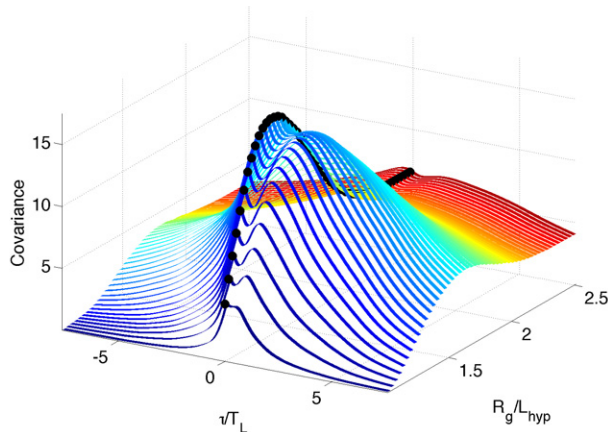


Fig. 8: (Color online) Cross-covariance of  $\Delta_{hyp}$ , the distance to the nearest hyperbolic point, and the triangle growth rate averaged over an ensemble of triangles, conditioned on  $R_g/L_{hyp}$ . The black dots show the covariance for  $\tau/T_L = 0$ .

and  $dR_g/dt$  are well correlated, but with the strongest correlation coming with a characteristic lag after the triangle passes the hyperbolic point. We associate this lag with the low flow velocities just around a hyperbolic point (since it is a stagnation point): the triangle vertices must be advected slightly away from the hyperbolic point itself before they can separate quickly. Second, the covariance is strongest for triangles whose size is on the order of the mean hyperbolic point spacing,  $R_g \sim 1.4L_{hyp}$ . This shows that triangles larger than the scale of the critical-point separation do not contribute to this effect.

**Conclusions.** – By studying the shape dynamics of Lagrangian triangles, we have elucidated the mechanisms that govern the distortion of material volumes in complex flow. The process by which triangles grow and deform consists of a sequence of distinct phases. Triangles are first caught in coherently straining regions and become nearly collinear. Subsequently, they grow rapidly until one vertex separates from the other two, though in a random direction. Finally, the two close vertices also separate, the dynamics of the three points decorrelates, and the shape distribution is identical to that of random triplets in two-dimensional space. The situation is qualitatively different for diffusively evolving triangles, where there is no coherent strain.

We expect that the qualitative results here are likely to be quite generic, and thus may also apply to three-dimensional turbulent flows, which also show non-trivial shape dynamics [2,3,6,8], with two principle distinctions: coherent straining regions are not quasi-one-dimensional in three-dimensional turbulence, and Lagrangian points separate algebraically rather than exponentially. By properly accounting for these distinctions, however, the general mechanisms outlined here may potentially be used to refine turbulence models that depend on material-volume deformation.

\*\*\*

This work was supported by the US National Science Foundation under Grant No. DMR-0906245.

## REFERENCES

- [1] SHRAIMAN B. I. and SIGGIA E. D., *Nature*, **405** (2000) 639.
- [2] CHERTKOV M., PUMIR A. and SHRAIMAN B. I., *Phys. Fluids*, **11** (1999) 2394.
- [3] PUMIR A., SHRAIMAN B. I. and CHERTKOV M., *Phys. Rev. Lett.*, **85** (2000) 5324.
- [4] CELANI A. and VERGASSOLA M., *Phys. Rev. Lett.*, **86** (2001) 424.
- [5] PUMIR A., SHRAIMAN B. I. and CHERTKOV M., *Europhys. Lett.*, **56** (2001) 379.
- [6] BIFERALE L., BOFFETTA G., CELANI A., DEVENISH B. J., LANOTTE A. and TOSCHI F., *Phys. Fluids*, **17** (2005) 111701.
- [7] LÜTHI B., OTT S., BERG J. and MANN J., *J. Turbul.*, **8** (2007) N45.
- [8] XU H., OUELLETTE N. T. and BODENSCHATZ E., *New J. Phys.*, **10** (2008) 013012.
- [9] MERRIFIELD S. T., KELLEY D. H. and OUELLETTE N. T., *Phys. Rev. Lett.*, **104** (2010) 254501.
- [10] KELLEY D. H. and OUELLETTE N. T., *Nat. Phys.*, **7** (2011) 477.
- [11] KELLEY D. H. and OUELLETTE N. T., *Phys. Fluids*, **23** (2011) 045103.
- [12] PARET J., MARTEAU D., PAIREAU O. and TABELING P., *Phys. Fluids*, **9** (1997) 3102.
- [13] CASTIGLIONE P. and PUMIR A., *Phys. Rev. E*, **64** (2001) 056303.
- [14] VOTH G. A., HALLER G. and GOLLUB J. P., *Phys. Rev. Lett.*, **88** (2002) 254501.
- [15] RIVERA M. K. and ECKE R. E., *Phys. Rev. Lett.*, **95** (2005) 194503.
- [16] OUELLETTE N. T. and GOLLUB J. P., *Phys. Rev. Lett.*, **99** (2007) 194502.
- [17] OUELLETTE N. T. and GOLLUB J. P., *Phys. Fluids*, **20** (2008) 064104.
- [18] OUELLETTE N. T., XU H. and BODENSCHATZ E., *Exp. Fluids*, **40** (2006) 301.
- [19] MORDANT N., CRAWFORD A. M. and BODENSCHATZ E., *Physica D*, **193** (2004) 245.
- [20] LEKIEN F., COULLIETTE C., BANK R. and MARSDEN J., *J. Geophys. Res.*, **109** (2004) C12004.
- [21] BERG J., OTT S., MANN J. and LÜTHI B., *Phys. Rev. E*, **80** (2009) 026316.
- [22] OUELLETTE N. T., O'MALLEY P. J. J. and GOLLUB J. P., *Phys. Rev. Lett.*, **101** (2008) 174504.
- [23] SHRAIMAN B. I. and SIGGIA E. D., *Phys. Rev. E*, **57** (1998) 2965.
- [24] PUMIR A., *Phys. Rev. E*, **57** (1998) 2914.
- [25] KHAN M. A. I., PUMIR A. and VASSILICOS J. C., *Phys. Rev. E*, **68** (2003) 026313.
- [26] HALLER G. and YUAN G., *Physica D*, **147** (2000) 352.
- [27] PARSA S., GUASTO J. S., KISHORE M., OUELLETTE N. T., GOLLUB J. P. and VOTH G. A., *Phys. Fluids*, **23** (2011) 043302.
- [28] JANA S. C. and OTTINO J. M., *Philos. Trans. R. Soc. London, Ser. A*, **338** (1992) 519.